

# Anatomy of inclusive $t\bar{t}W$ production at hadron colliders

Stefan von Buddenbrock<sup>a</sup>, Richard Ruiz<sup>b</sup>, Bruce Mellado<sup>a,c</sup>

<sup>a</sup>*School of Physics and Institute for Collider Particle Physics, University of the Witwatersrand, Wits, Johannesburg 2050, South Africa*

<sup>b</sup>*Centre for Cosmology, Particle Physics and Phenomenology (CP3), Université catholique de Louvain, Chemin du Cyclotron, Louvain-la-Neuve, B-1348, Belgium*

<sup>c</sup>*iThemba LABS, National Research Foundation, PO Box 722, Somerset West 7129, South Africa*

## Abstract

In LHC searches for new and rare phenomena the top-associated channel  $pp \rightarrow t\bar{t}W^\pm + X$  is a challenging background that multilepton analyses must overcome. Motivated by sustained measurements of enhanced rates of same-sign and multi-lepton final states, we reexamine the importance of higher jet multiplicities in  $pp \rightarrow t\bar{t}W^\pm + X$  that enter at  $\mathcal{O}(\alpha_s^3\alpha)$  and  $\mathcal{O}(\alpha_s^4\alpha)$ , i.e., that contribute at NLO and NNLO in QCD in inclusive  $t\bar{t}W^\pm$  production. Using fixed-order computations, we estimate that a mixture of real and virtual corrections at  $\mathcal{O}(\alpha_s^4\alpha)$  in well-defined regions of phase space can arguably increase the total  $t\bar{t}W^\pm$  rate at NLO by at least 10% – 14%. However, by using non-unitary, NLO multi-jet matching, we estimate that same these corrections are at most 10% – 12%, and at the same time exhibit the enhanced jet multiplicities that are slightly favored by data. This seeming incongruity suggests a need for the full NNLO result. We comment on implications for the  $t\bar{t}Z$  process.

**Keywords:** Top Quarks, Jet Matching, Large Hadron Collider

## 1. Introduction

The discovery [1, 2] of the  $pp \rightarrow t\bar{t}W$  process, and likewise  $pp \rightarrow t\bar{t}Z$ , is an important milestone of the Large Hadron Collider’s (LHC’s) Standard Model (SM), Higgs, and New Physics programs. In its own right,  $t\bar{t}W$ , which at lowest order proceeds at  $\mathcal{O}(\alpha_s^2\alpha)$  through the diagrams in figure 1, is a multi-scale process with large quantum chromodynamic (QCD) and electroweak (EW) corrections. Hence, it is a laboratory for stress-testing the SM paradigm. At the same time, the  $t\bar{t}W^\pm \rightarrow W^+W^-W^\pm b\bar{b}$  decay mode can give rise to the same-sign dilepton  $\ell_i^\pm \ell_j^\pm$  and trilepton  $\ell_i \ell_j \ell_k$  signal categories, encumbering [3, 4, 5, 6] searches for lepton number and lepton flavor violation as well as measurements of the Higgs’s couplings.

Motivated by this major efforts have been undertaken since the top’s discovery to reliably describe the  $t\bar{t}W/Z$  processes. This includes QCD corrections to production and decay modes up to next-to-leading order (NLO) with parton shower (PS) matching [4, 7, 8, 9, 10, 11, 12, 13, 14, 15, 16, 17, 18]; soft gluon resummation up to next-to-next-to-leading logarithm (NNLL) in perturbative QCD [19, 20, 21] and effective field theory [22, 23, 24, 25]; EW corrections up to NLO [25, 26, 27, 28, 29], as well as their systematic merger with QCD corrections [25, 27, 29, 30].

The findings are telling: Known QCD corrections increase total LHC rates by 20% – 60%, depending on theoretical inputs, and reflect the 15% – 85% scale ambiguity at leading order (LO). Even at this level, however, typical scale choices leave an 10% – 30% uncertainty, suggesting additional corrections are

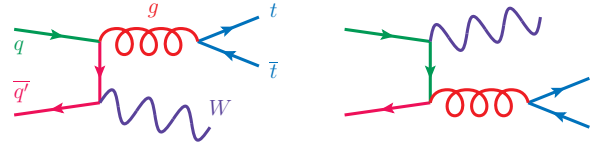


Figure 1: Lowest order, Born-level diagram for the  $q\bar{q} \rightarrow t\bar{t}W^\pm$  process.

needed to ensure theoretical control. While EW corrections increase rates by a net 5%, uncertainties essentially stay the same.

In comparison to data, a consistent picture has also emerged: Whereas first observations of the  $t\bar{t}Z$  process by the ATLAS and CMS collaborations at  $\sqrt{s} = 8$  TeV were within SM expectations at NLO in QCD, both collaborations measured a  $t\bar{t}W$  rate exceeding predictions at the 68% ( $1\sigma$ ) confidence level (CL) [1, 2]. Measurements at  $\sqrt{s} = 13$  TeV with up to  $\mathcal{L} \approx 36$  fb<sup>-1</sup> support a  $t\bar{t}W$  rate that is 15% – 50% larger than predictions at NLO in QCD at about the same CL tension [31, 32, 33]; a modest  $t\bar{t}Z$  rate increase of 15% is also preferred [31]. Improved measurements with  $\mathcal{L} \approx 80$  fb<sup>-1</sup> [34] and  $\mathcal{L} \approx 140$  fb<sup>-1</sup> [35, 36] affirm a  $t\bar{t}W$  rate that, depending on the signal category, is 25% – 70% larger than predictions at NLO in QCD and EW, and corresponds to a  $1.4\sigma$  –  $2.4\sigma$  discrepancy. Given the sustained nature of these and other multilepton excesses, which include a diverse number of final states that are dominated by several SM processes, it is reasonable to contemplate seriously the possible role of new physics [37, 38, 39, 40]. That said, it is also necessary to investigate each anomaly separately to understand the possible importance of missing higher order corrections.

To support such investigations and to exhaust possible SM explanations we have reexamined the role of the  $t\bar{t}W^\pm j$  and

stef.von.b@cern.ch (Stefan von Buddenbrock),  
richard.ruiz@uclouvain.be (Richard Ruiz),  
Bruce.Mellado.Garcia@cern.ch (Bruce Mellado)

$t\bar{t}W^\pm jj$  sub-processes at  $O(\alpha_s^3\alpha)$  and  $O(\alpha_s^4\alpha)$  in inclusive  $t\bar{t}W$  production. While complementary works have studied the phenomenology of these channels [4, 15, 17], the impact on the inclusive cross section were not among their intents.

As a first step we use fixed order computations and find that a subset of well-defined real and virtual contributions at  $O(\alpha_s^4\alpha)$ , i.e., finite elements to inclusive  $t\bar{t}W$  production at next-to-next-to-leading order (NNLO) in QCD, are positive and reach at least 10% – 14% of the  $t\bar{t}W^\pm$  rate at NLO. Interestingly, we find that these same contributions only increase the  $t\bar{t}W$  rate by at most 10% – 12% when using then the non-unitary, NLO multi-jet matching procedure FxFx [41]. Despite this seeming discrepancy, we report that after imposing selection cuts and signal categorizations employed LHC experiments, the FxFx results exhibit enhanced light and heavy jet multiplicities that are slightly favored by data. To resolve this enigma, we argue a need for the full NNLO in QCD description of inclusive  $t\bar{t}W$  production.

The report of our investigation continues as follows: After summarizing our computational setup in section 2, we build up the anatomy of inclusive  $t\bar{t}W$  production at hadron colliders in section 3. There we estimate higher order corrections to  $t\bar{t}W$  production and discuss theoretical uncertainties. In section 4, we show how rate increases propagate to differential observables and survive analysis cuts. In section 5, we present an outlook for the  $t\bar{t}Z$  process. We conclude in section 6.

## 2. Computational Setup

To conduct our study we employ a state-of-the-art simulation tool chain based on Monte Carlo methods. For matrix element evaluation and parton-level event generation, we use MadGraph5\_aMC@NLO (v2.6.7) [15] (mg5amc). Its conglomeration of packages [42, 43, 44, 45, 46, 47] enables us to simulate high- $p_T$  hadron collisions in the SM up to NLO in QCD with PS-matching within the MC@NLO formalism [42]. We model decays of heavy resonances using the spin-correlated narrow width approximation [45, 46]. Parton-level events are passed through Pythia8 (v244) [48] for QCD and QED parton showering, hadronization, and modeling the underlying event. We use the FxFx prescription [41] as implemented in mg5amc. Parton-level sequential clustering is handled according to  $k_T$ -class algorithms [49, 50, 51] as implemented in FastJet [52, 53]. To compare against ATLAS  $t\bar{t}W$  results at  $\sqrt{s} = 13$  TeV [34], events are processed with DELPHES3 (v3.4.2) [54] to model detector resolution. We assume most of the default settings for the ATLAS detector card. However, to better mimic ATLAS’s analysis we employ updated lepton and  $b$ -tagging efficiencies [55, 56, 57].

Throughout this analysis, we work in the  $n_f = 4$  active quark flavor scheme with SM inputs as set by the mg5amc module loop\_sm. We do so for a more realistic description of massive  $B$  hadrons decays, and particularly charged lepton multiplicities. We tune the top and Higgs masses to

$$m_t(m_t) = 172.9 \text{ GeV} \quad \text{and} \quad m_H = 125.1 \text{ GeV}. \quad (1)$$

For all computations we use the NNPDF 3.1 NNLO parton density functions (PDFs) (1haid=303600) [58] as evaluated by

LHAPDF (v6.2.3) [59]. PDF uncertainties are obtained via the replica method [59, 58]. We take as our central ( $\zeta = 1$ ) collinear factorization ( $\mu_f$ ) and QCD renormalization ( $\mu_r$ ) scales half the sum over final-state transverse energies,

$$\mu_f, \mu_r = \zeta \times \frac{\tilde{H}_T}{2}, \quad \tilde{H}_T \equiv \sum_{k=i,\bar{i},W^\pm,j} \sqrt{m_k^2 + p_{T,k}^2}. \quad (2)$$

The shower scale  $\mu_s$  is kept at its default value [15]. For FxFx computations, scales are set according to Refs. [41, 46]. Uncertainties associated with  $\mu_f, \mu_r$ , and  $\mu_s$  are estimated by rescaling them individually by  $\zeta \in [0.5, 1, 2.0]$ .

## 3. Anatomy of inclusive $t\bar{t}W$ production at the LHC

It may be that sustained measurements [31, 32, 33, 36, 34, 35] of a  $t\bar{t}W$  cross section that is larger than expectations at NLO in QCD and EW is due to new physics. As such, we find it compelling to exhaust SM explanations for these observations. In this context, we review in section 3.1 the modeling and uncertainties of  $t\bar{t}W$  production at various orders in perturbation theory. Motivated by our findings, we turn our focus in section 3.2 to the  $t\bar{t}Wj$  and  $t\bar{t}Wjj$  subprocesses and their roles in the inclusive channel. We then present in section 3.3 our estimations for the  $t\bar{t}W$  production rate at the level of NLO multi-jet matching. Differential results are presented in section 4.

### 3.1. State-of-the-art modeling for inclusive production

Categorically, the anatomy of inclusive  $t\bar{t}W$  production consists of several pieces and nuances. To start: at lowest order, i.e., at  $O(\alpha_s^2\alpha)$ , cross sections at the  $\sqrt{s} = 13$  TeV LHC span  $\sigma_{t\bar{t}W}^{\text{LO}} \sim 375 \text{ fb} - 525 \text{ fb}$ , depending on choices for PDF and  $\mu_f, \mu_r$ . The normalization of  $\alpha_s(\mu_r)$  heavily influences the outcome. For static scale choices of  $\mu_f, \mu_r \sim O(m_t)$ , 3- or 9-point scale variation reveals an ambiguity of 25%–35% [11]. For typical dynamic choices, such as equation 2, one finds comparable uncertainties of 20%–30% but rates that are about 25% smaller [15, 16, 4]. The same holds for static choices of  $O(2m_t + M_W)$ , indicating that the threshold and kinematic scales are similar.

At NLO in QCD, contributions at  $O(\alpha_s^3\alpha)$  improve the picture dramatically. Due to the opening of ( $qg$ )-scattering, cross sections jump by 20% – 50%, again depending on inputs, to  $\sigma_{t\bar{t}W}^{\text{NLO}} \sim 485 \text{ fb} - 645 \text{ fb}$  [4, 11, 15, 16, 20]. Excluding scale choices that favor values far below  $O(2m_t + M_W)$ , rates more moderately span  $\sigma_{t\bar{t}W}^{\text{NLO}} \sim 485 \text{ fb} - 595 \text{ fb}$ . However, the range does not reflect scale variation, which spans only 10% – 15%, and suggests that further high-order corrections are needed to ensure theoretical control. This is partly due to the ( $qg$ )-scattering channel, which at this level only is described at LO.

Beyond leading contributions at  $O(\alpha_s^2\alpha)$  and  $O(\alpha_s^3\alpha)$ , it is now known [26, 27, 28] that “supposedly” sub-leading EW contributions at the Born level, i.e., at  $O(\alpha^3)$ , and at NLO, i.e., at  $O(\alpha_s^2\alpha^2)$ ,  $O(\alpha_s\alpha^3)$ , and  $O(\alpha^4)$ , are not negligible in comparison to the above uncertainty budget. Cancellations among virtual EW diagrams, interference between mixed EW-QCD and pure

EW diagrams, real radiation, and the opening of  $tW \rightarrow tW$  scattering, culminate in a positive contribution to  $t\bar{t}W$  production that is about 6% of the rate at NLO in QCD [28]:

$$K_{\text{NLO-EW}} = \sigma^{\text{NLO-EW+NLO-QCD}} / \sigma^{\text{NLO-QCD}} = 1.06. \quad (3)$$

Despite these improvements, dynamic scale variation at this order remains about the same as at NLO in QCD.

First attempts to extract two-loop predictions through resumming soft gluon radiation in the  $q\bar{q} \rightarrow t\bar{t}W$  channel up to NNLL yield positive corrections [20, 21, 22, 23, 24, 25]. Depending on scale inputs, these range 1% – 7% and reduce slightly both the scale uncertainty and range of predictions [20].

In one<sup>1</sup> detailed comparison to data [34], measurements of the  $t\bar{t}W$  cross section by ATLAS with  $\mathcal{L} \approx 80 \text{ fb}^{-1}$  at  $\sqrt{s} = 13 \text{ TeV}$  find category-based signal strengths that are 25%–70% larger than SM expectations. Relative to the SM prediction of  $\sigma_{t\bar{t}W}^{\text{ATLAS-TH.}} = 727 \text{ fb}^{+13\%}_{-13\%}$ , the measurements indicate a best-fit rate and signal strength of [34],

$$\hat{\sigma}_{t\bar{t}W}^{\text{ATLAS-EX.}} = 1010 \text{ fb}^{+12\%}_{-12\%}, \quad \hat{\lambda}_{t\bar{t}W}^{\text{ATLAS-EX.}} = 1.39^{+0.17}_{-0.16}, \quad (4)$$

which corresponds to a  $2.4\sigma$  discrepancy. Importantly, the prediction is built from an established [5] reference point with leading QCD and EW corrections,  $\sigma_{t\bar{t}W}^{\text{ref.}} = 601 \text{ fb}^{+13\%}_{-12\%}$ , accounts for additional EW corrections [28] through a scaling factor  $K_{\text{sub-NLO-EW}} = 1.09$ , but also includes a scaling factor  $K_{\text{NNLO-QCD}}^{\text{est.}} = 1.11$  for NNLO in QCD contributions.

While seemingly innocuous, the estimate of  $K_{\text{NNLO-QCD}}^{\text{est.}}$  is based on the observation [15] that the  $pp \rightarrow t\bar{t}Wj$  process exhibits a large,  $\mathcal{O}(40\%)$  correction at NLO in QCD for a specific set of inputs. However, neither Ref. [15] nor follow-up work [4] evaluate the  $t\bar{t}W$  rate beyond  $\mathcal{O}(\alpha_s^3\alpha)$ . Therefore, owing to the uncertainty in  $K_{\text{NNLO-QCD}}^{\text{est.}}$ , we turn our focus to the roles of the  $t\bar{t}Wj$  and  $t\bar{t}Wjj$  subprocesses in inclusive  $t\bar{t}W$  production.

### 3.2. The $t\bar{t}Wj$ and $t\bar{t}Wjj$ processes

To investigate the  $pp \rightarrow t\bar{t}Wj$  and  $pp \rightarrow t\bar{t}Wjj$  processes, we argue first for definitions of these channels that ensure their matrix elements (MEs) are perturbative in the CSS sense [60, 61], i.e., are absent of large collinear logarithms. Such logarithms originate from real radiation that goes soft or collinear and require sufficiently stringent transverse momentum cuts ( $p_T^{j \text{ min}}$ ) to render MEs physical. For a ( $t\bar{t}W$ )-system invariant mass of  $M_{t\bar{t}W}$ , these contributions cause cross sections to scale as

$$\sigma(pp \rightarrow t\bar{t}W^\pm + nj) \sim \sum_{k=n} \alpha_s^k (p_T^{j \text{ min}}) \log^{2k-1} \left( \frac{M_{t\bar{t}W}^2}{p_T^{j \text{ min}} 2} \right). \quad (5)$$

For too small  $p_T^{j \text{ min}}$  one enters the Sudakov regime where log factors exceed  $1/\alpha_s$  factors and  $k_T$ -resummation is needed.

To establish a sufficiently “safe”  $p_T^{j \text{ min}}$ , we consider at  $\sqrt{s} = 13 \text{ TeV}$  the  $pp \rightarrow t\bar{t}W$  process at NLO in QCD, i.e., up to  $\mathcal{O}(\alpha_s^3\alpha)$ , and the LO decay to charged leptons,

$$pp \rightarrow t\bar{t}W^\pm \rightarrow 3W b\bar{b} \rightarrow 3\ell 3\nu b\bar{b}, \quad \ell \in \{e, \mu\}. \quad (6)$$

<sup>1</sup>Other measurements at  $\sqrt{s} = 13 \text{ TeV}$  [31, 32, 33, 36, 34, 35] show similar disagreements but provide fewer modeling details.

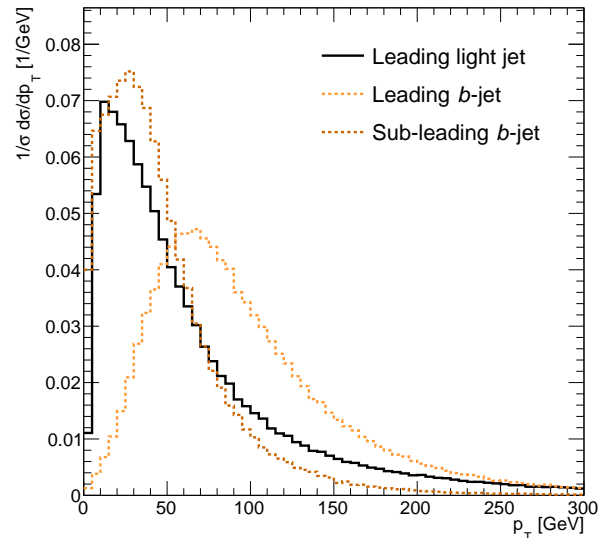


Figure 2: Normalized  $p_T$  distributions of the leading  $b$ -jet (light dash), sub-leading  $b$ -jet (dark dash), and leading light jet (solid) in the  $pp \rightarrow t\bar{t}W \rightarrow 3\ell + X$  process at NLO in QCD with PS matching.

Here and throughout we choose the dynamic scale scheme of equation 2 following studies [62, 63] of the  $pp \rightarrow W + nj$  process. There, schemes not reflective of kinematic scales were shown to lead to negative cross sections at NLO. For the inclusive  $t\bar{t}W$  process at NLO (LO) in QCD, we obtain

$$\sigma_{t\bar{t}W^\pm}^{\text{NLO-QCD (LO)}} = 594 \text{ fb}^{+11\%}_{-10\%} {}^{+2.0\%}_{-2.0\%} (378 \text{ fb}^{+24\%}_{-18\%} {}^{+2.2\%}_{-2.2\%}), \quad (7)$$

as our baseline NLO (LO) cross sections. Uncertainties reflect scale and PDF dependence, respectively.

After parton showering, anti- $k_T$  clustering ( $R = 0.4$ ), and overlap removal between leptons and jets, we plot in figure 2 the normalized  $p_T$  distribution of the leading light jet (solid). As a check of our computational setup, we also plot the leading (light dash) and sub-leading (dark dash)  $b$ -jet. The  $b$ -jet distributions reflect the characteristic momentum  $p_T \sim m_t(1 - M_W^2/m_t^2)/2 \sim 65 \text{ GeV} - 70 \text{ GeV}$ , modulo recoils against  $W$  and light jets.

Since the  $t\bar{t}W$  system is fully decayed to leptons, the leading light jet is an  $\mathcal{O}(\alpha_s^3\alpha)$  contribution that originates in the MC@NLO formalism [42] from (i) the tree-level  $t\bar{t}Wj$  ME at “large” ( $p_T^j/M_{t\bar{t}W}$ ) or (ii) PS corrections to the one-loop-improved  $t\bar{t}W$  ME at “small” ( $p_T^j/M_{t\bar{t}W}$ ). Using the procedure in Ref. [64], which generalizes an analogous procedure in Ref. [60], we estimate that the transition between the two domains occurs at around  $p_T^{\text{safe}} \sim 30 \text{ GeV}$  for  $M_{t\bar{t}W} \sim 425 \text{ GeV} - 475 \text{ GeV}$ . Notably, this estimate neglects  $\beta_0$  factors in  $\alpha_s$  running. Accounting for this we obtain instead  $p_T^{\text{safe}} \sim 95 \text{ GeV} - 100 \text{ GeV}$ . In comparison to figure 2 one sees that the transition occurs somewhere<sup>2</sup> between the Sudakov peak at  $p_T \sim 15 \text{ GeV} - 20 \text{ GeV}$  and  $p_T \sim 75 \text{ GeV} - 100 \text{ GeV}$ , with an

<sup>2</sup>For comparison, the Sudakov peak for  $W$  production occurs at  $p_T = 3 \text{ GeV} - 4 \text{ GeV}$ , is estimated to transition to fixed order MEs at  $p_T \sim 7 \text{ GeV} - 8 \text{ GeV}$  [60], and does so at  $p_T \sim 5 \text{ GeV} - 10 \text{ GeV}$  [65].

Order	$p_T^{j \min}$	$\sigma$ [fb]	$\pm\delta_{\mu_f, \mu_r}$	$\pm\delta_{\text{PDF}}$	$K_{\text{QCD}}$	$\Delta\sigma$ [fb]
LO	30 GeV	227	+40%	+1.3%	...	...
	40 GeV	191	-27%	-1.3%	...	...
	50 GeV	164	+41%	+1.3%	...	...
	75 GeV	122	-27%	-1.2%	...	...
	100 GeV	93.5	+42%	+1.1%	...	...
	125 GeV	74.5	-28%	-1.1%	...	...
	150 GeV	59.8	+43%	+1.3%	...	...
NLO	30 GeV	351	-28%	-1.1%	1.55	124
	40 GeV	303	+12%	+1.2%	1.59	112
	50 GeV	267	-14%	-1.2%	1.62	103
	75 GeV	205	+13%	+1.1%	1.68	83.0
	100 GeV	159	-14%	-1.0%	1.70	65.7
	125 GeV	129	+15%	+1.0%	1.73	54.7
	150 GeV	104	-16%	-0.9%	1.73	43.9

Table 1: Total cross sections [fb] at  $\sqrt{s} = 13$  TeV of the  $pp \rightarrow t\bar{t}W^\pm j$  process at LO and NLO in QCD, with scale and PDF uncertainties [%] for representative jet  $p_T$  thresholds ( $p_T^{j \min}$ ) with  $|\eta^j| < 4.0$ . Also shown are the  $K$ -factors and differences between NLO and LO rates.

inflection point at  $p_T \sim 50$  GeV. This is also roughly the geometric mean of the estimated  $p_T^{\text{safe}}$ . This suggests that regulators below  $p_T^{j \min} \sim 30$  GeV – 50 GeV will lead to unphysical MEs, intermediate cutoffs of  $p_T^{j \min} \sim 50$  GeV – 75 GeV can arguably stabilize MEs, but cutoffs at  $p_T^{j \min} \gtrsim 100$  GeV are fine.

To check this, for representative  $p_T^{j \min}$  with  $|\eta^j| < 4.0$ , we compute and list in table 1 cross sections at LO and NLO in QCD, i.e., up to  $\mathcal{O}(\alpha_s^3\alpha)$  and  $\mathcal{O}(\alpha_s^4\alpha)$ , for the process

$$pp \rightarrow t\bar{t}W^\pm j, \quad (8)$$

with scale and PDF uncertainties, the QCD  $K$ -factor

$$K_{\text{QCD}} \equiv \sigma^{\text{N}^{k+1}\text{LO}} / \sigma^{\text{N}^k\text{O}}, \quad (9)$$

and the difference between cross sections at NLO and LO

$$\Delta\sigma \equiv \sigma_{t\bar{t}Wj}^{\text{NLO}} - \sigma_{t\bar{t}Wj}^{\text{LO}}, \quad (10)$$

which quantifies  $\mathcal{O}(\alpha_s^4\alpha)$  contributions. For  $p_T^{j \min} = 30$  GeV – 150 GeV, NLO rates span  $\sigma_{t\bar{t}Wj}^{\text{NLO}} \sim 100$  fb – 350 fb, in agreement with Refs. [4, 15]. We report that scale uncertainties are uniform across  $p_T^{j \min}$  and reduce from 30% – 40% at LO to 15% at NLO, suggesting stability for  $p_T^{j \min} \gtrsim 50$  GeV – 75 GeV.

Two notable observations can be drawn from these rates. First is the size of the pure  $\mathcal{O}(\alpha_s^4\alpha)$  contributions. For  $p_T^{j \min} = 75$  GeV – 150 GeV, these are positive and span about  $\Delta\sigma \sim 45$  fb – 85 fb. In comparison to the baseline  $t\bar{t}W$  cross section in equation 7, we find that  $\Delta\sigma$  is 10% – 20% of the baseline rate at LO and 7% – 14% at NLO for our range of  $p_T^{j \min}$ . Specifically for  $p_T^{j \min} = 75$  GeV – 125 GeV, we find that  $\Delta\sigma$  alone is about 20% – 30% of the discrepancy reported in equation 4. The largeness of  $\Delta\sigma$  is despite the fact that it constitutes  $\mathcal{O}(\alpha_s^2)$  corrections to inclusive  $t\bar{t}W$  production, which would otherwise suggest that  $\Delta\sigma$  are at most  $\mathcal{O}(1 - 10\%)$ .

Importantly,  $\Delta\sigma$  encapsulates corrections to  $t\bar{t}Wj$  for a leading jet  $j_1$  that is well-defined in the CSS sense; it does not reflect

$ij \rightarrow t\bar{t}W^\pm kl$							
$(i, j)$	$(k, l)$	$p_T^{j_1 \min}$	$p_T^{j_2 \min}$	$\sigma$ [fb]	$\pm\delta_{\mu_f, \mu_r}$	$\pm\delta_{\text{PDF}}$	
All	All	75 GeV	75 GeV	34.7 (100%)	+57%	+1.1%	
$(g, g)$	$(g, Q)$			23.7 (68%)	-34%	-1.1%	
$(Q, Q)$	$(Q, Q)$			6.99 (20%)			
$(Q, Q)$	$(g, g)$			3.63 (10%)			
$(g, g)$	$(q, \bar{q})$			0.437 (1.3%)			
All	All	100 GeV	75 GeV	33.1 (100%)	+57%	+1.0%	
$(g, Q)$	$(g, Q)$			22.6 (68%)	-34%	-1.0%	
$(Q, Q)$	$(Q, Q)$			6.78 (20%)			
$(Q, Q)$	$(g, g)$			3.28 (9.9%)			
$(g, g)$	$(q, \bar{q})$			0.409 (1.2%)			
All	All	100 GeV	100 GeV	21.2 (100%)	+57%	+1.1%	
$(g, Q)$	$(g, Q)$			14.3 (67%)	-34%	-1.1%	
$(Q, Q)$	$(Q, Q)$			4.91 (23%)			
$(Q, Q)$	$(g, g)$			1.75 (8%)			
$(g, g)$	$(q, \bar{q})$			2.58 (1%)			
$(g, qv)$	$(g, qv)$	75 GeV	75 GeV	20.1 (58%)	+58%	+2.3%	
$(g, qv)$	$(g, qv)$	100 GeV	75 GeV	19.3 (58%)	-35%	-2.3%	
$(g, qv)$	$(g, qv)$	100 GeV	100 GeV	12.2 (58%)	+59%	+2.4%	
					-35%	-2.4%	

Table 2: Total cross sections [fb] at  $\sqrt{s} = 13$  TeV for the  $pp \rightarrow t\bar{t}W^\pm jj$  process at LO, with scale and PDF uncertainties [%], for representative  $p_T^{j_1 \min}$  with  $|\eta^j| < 4.0$ . Also shown is the decomposition according to partonic channel, for  $qv \in \{u, d\}$ ,  $q \in \{u, d, c, s\}$ , and  $Q \in \{q, \bar{q}\}$ .

corrections for when  $j_1$  is in the soft-wide angle limit. Extrapolating from table 1 hints that such corrections remain positive and that the  $K_{\text{NNLO-QCD}}^{\text{est}}$  in the previous section underestimates NNLO in QCD corrections by at least a factor of two. Isolating this, however, is complicated by the phase space region where  $j_1$  is hard but collinear to the beam line, which cancels against negative-valued PDF/collinear counter terms at NNLO.

The second observation is that QCD corrections to the  $t\bar{t}Wj$  process are large, with  $K$ -factors ranging  $K_{\text{QCD}} \sim 1.7$  for  $p_T^{j \min} = 75$  GeV – 150 GeV, and with the largest (smallest)  $p_T^{j \min}$  exhibiting the largest (smallest) corrections. In analogy to  $t\bar{t}W$ , it is possible that new partonic channels associated with the  $t\bar{t}Wjj$  sub-process at  $\mathcal{O}(\alpha_s^4\alpha)$  drive these increases.

To check this we consider at LO, i.e.,  $\mathcal{O}(\alpha_s^4\alpha)$ , the channel

$$pp \rightarrow t\bar{t}W^\pm jj, \quad (11)$$

and list in table 2 the  $\sqrt{s} = 13$  TeV cross sections [fb] with uncertainties [%], for benchmark  $p_T^{j_1 \min}$  on the leading ( $j_1$ ) and sub-leading ( $j_2$ ) jets, and with  $|\eta^j| < 4.0$ . Also shown is the decomposition according to initial/final-state partons.

For  $p_T^{j_1 \min} = 75$  GeV, 100 GeV, we find that rates span  $\sigma_{t\bar{t}Wjj}^{\text{LO}} \sim 20$  fb – 35 fb, with up to 60% scale uncertainty and about a 1% PDF uncertainty. This translates to about 5% – 9% (3% – 6%) of the baseline  $t\bar{t}W$  rate at (N)LO. For all cases, quark-gluon scattering ( $Q, g$ ) accounts for about 70% of the total  $t\bar{t}Wjj$  rate, whereas quark-quark scattering ( $Q, Q$ ) contributes 20%. This effectively rules out enhancements to  $t\bar{t}W$  production at NNLO from valence-valence scattering. Instead, we find evidence of a large gluon-valence component, with 60% of the  $t\bar{t}Wjj$  rate being due to gluon-up/down scattering ( $g, qv$ ).

Returning to  $\Delta\sigma$  in equation 10, we recall that it encapsulates the  $\mathcal{O}(\alpha_s^4\alpha)$  parts of  $t\bar{t}Wj$  production at NLO in QCD. Given then the LO  $t\bar{t}Wjj$  rate, we can estimate the net impact of the

soft-real, virtual, and counter-term corrections (SR+V+CT) to  $t\bar{t}Wj$  by taking the difference of the two:

$$\Delta\sigma_{t\bar{t}Wj}^{\text{SR+V+CT}}(p_T^{j_1 \min}, p_T^{j_2 \min}) \equiv \Delta\sigma_{t\bar{t}Wj}(p_T^{j_1 \min}) - \sigma_{t\bar{t}Wj}^{\text{LO}}(p_T^{j_1 \min}, p_T^{j_2 \min}). \quad (12)$$

After doing so, we find that the absolute [fb] (relative [%]) unresolved corrections to the  $t\bar{t}Wj$  process at NLO are

$$\Delta\sigma_{t\bar{t}Wj}^{\text{SR+V+CT}}(75 \text{ GeV}, 75 \text{ GeV}) = +48.3 \text{ fb (+58\%)}, \quad (13a)$$

$$\Delta\sigma_{t\bar{t}Wj}^{\text{SR+V+CT}}(100 \text{ GeV}, 75 \text{ GeV}) = +32.6 \text{ fb (+50\%)}, \quad (13b)$$

$$\Delta\sigma_{t\bar{t}Wj}^{\text{SR+V+CT}}(100 \text{ GeV}, 100 \text{ GeV}) = +44.5 \text{ fb (+68\%)}. \quad (13c)$$

For  $p_T^{j_1 \min} = p_T^{j_2 \min} = 75 \text{ GeV} - 100 \text{ GeV}$ , we find that SR+V+CT corrections constitute about 60%–70% of  $\Delta\sigma$ . This suggests that the  $\mathcal{O}(\alpha_s^4\alpha)$  contributions at  $p_T^{j_k \min} = 75(100) \text{ GeV}$  are dominated by unresolved radiation. For mixed  $p_T^{j_k \min}$ , SR+V+CT corrections dip to 50%, demonstrating an interplay between resolved and unresolved radiation. (This includes the role of the hierarchy  $p_T^{j_1 \min} \gg p_T^{j_2 \min}$ , which introduces logarithmic structures not captured in equation 5 [66, 67].) Importantly, the interplay in equation 13 highlights that adding  $\Delta\sigma_{t\bar{t}Wj}$  at low  $p_T^{j \min}$  to inclusive  $t\bar{t}W$  should be accompanied by a reweighting / subtraction scheme that systematically protects against double counting of low- $p_T$  radiation.

In summary, we report the existence of partonic configurations at  $\mathcal{O}(\alpha_s^4\alpha)$ , i.e., pure  $\mathcal{O}(\alpha_s^2)$  corrections to inclusive  $t\bar{t}W$  production, with cross sections in well-defined phase space regions that greatly exceed estimates by standard scale variation at NLO in QCD. By one measure (table 1) a subset of these corrections span at least  $\Delta\sigma \sim 65 \text{ fb} - 85 \text{ fb}$ , or about 10%–14% of the inclusive rate at NLO in QCD, and follows from a mixture of gluon-valence scattering in  $t\bar{t}Wjj$  at LO (table 2) and unresolved radiation in  $t\bar{t}Wj$  at NLO (equation 13). While alone accounting for 20%–30% of the discrepancy in measured the  $t\bar{t}W$  rate at  $\sqrt{s} = 13 \text{ TeV}$  (see, for example, equation 4), other contributions at  $\mathcal{O}(\alpha_s^4\alpha)$ , such as two emissions of soft, wide-angle legs and one soft leg at one-loop, which are arguably positive, are not included. Importantly, resummed results at NNLL do not suggest large cancelations against pure two-loop diagrams. Guided by this, we turn to the impact of combining the  $t\bar{t}W$  and  $t\bar{t}Wj$  processes using NLO multi-jet matching.

### 3.3. Inclusive production with NLO multi-jet matching

As a complementary estimate of the  $\mathcal{O}(\alpha_s^4\alpha)$  contributions to  $t\bar{t}W$  production that stem from the  $t\bar{t}W + nj$  sub-channels, we employ the FxFx NLO multi-jet matching [41]. In short, FxFx is an established [68, 69, 70, 71], non-unitarity [41, 72] procedure within the MC@NLO formalism for promoting jet observables at LO+LL to NLO+LL through CKKW-like [73] reweighting. In particular, hard, wide-angle emissions are included through exact MEs at one-loop and double counting is avoided by Sudakov reweighting. As such, cross sections at NLO are augmented with terms that are  $\mathcal{O}(\alpha_s^2)$  or higher.

The cost of this improvement is the introduction of a merging scale ( $Q_{\text{cut}}^{\text{FxFx}}$ ) akin to those at LO. To set  $Q_{\text{cut}}^{\text{FxFx}}$  we follow Refs. [15, 41, 72], which call for  $Q_{\text{cut}}^{\text{FxFx}} > 2p_T^{j \min}$ . In

principle, FxFx merging is independent of  $p_T^{j \min}$  and ultra-low  $p_T^{j \min}$  choices simply lead to high event-veto rates and therefore poorer Monte Carlo efficiency. Formally, however, the Sudakov-reweighting in FxFx only cancels the collinear logarithms that are shared by MEs and the PS; for sufficiently small  $p_T^{j \min}$ , mis-cancellations of soft logarithms can technically spoil perturbative convergence. Therefore, as a jet  $p_T$  threshold is needed to regulate Born-level  $t\bar{t}W + nj$  MEs, we also require that  $p_T^{j \min}$  is not too low in the CSS sense and that  $|\eta^j| < 4.0$ . We match up to the first jet multiplicity (denoted as FxFx1j) and set as our baseline configuration

$$(p_T^{j \min}, Q_{\text{cut}}^{\text{FxFx}}) = (50 \text{ GeV}, 110 \text{ GeV}). \quad (14)$$

At this order we obtain as the inclusive  $t\bar{t}W$  cross section

$$\sigma_{t\bar{t}W^\pm}^{\text{FxFx1j}} = 655 \text{ fb}_{-12\% -1.6\%}^{+12\% +1.6\%}, \quad (15)$$

where the uncertainties reflect scale and PDF dependence, respectively. We report that corrections at this order increase the baseline NLO rate in equation 7 by about 10% with the size uncertainties remaining essentially the same. This is in agreement with the estimated [34]  $K_{\text{NNLO-QCD}}^{\text{est}} = 1.11$ , and hence is at odds with table 1, which suggests that such  $\mathcal{O}(\alpha_s^4\alpha)$  contributions are larger.

Accounting now for the EW corrections in equation 3 [28] and assuming the FxFx uncertainties above, we obtain

$$\sigma_{t\bar{t}W^\pm}^{\text{FxFx1j+EW}} \equiv \sigma_{t\bar{t}W^\pm}^{\text{FxFx1j}} + \delta\sigma_{\text{EW}}^{\text{NLO}} = 690 \text{ fb}_{-12\% -1.6\%}^{+12\% +1.6\%}, \quad (16)$$

We find that this rate is about 5% smaller than the prediction used in the ATLAS measurement of Ref. [34], and that the difference is mainly due to the scale and PDF choices in the baseline NLO in QCD rate. (A 1% difference follows from our FxFx correction being smaller than the estimated NNLO  $K$ -factor.) In principle, this revised cross section worsens slightly the discrepancy reported in equation 4. For the pure FxFx and FxFx+EW cases, the corresponding best-fit signal strengths are

$$\hat{\lambda}_{t\bar{t}W}^{\text{FxFx1j}} = 1.54_{-0.18}^{+0.19}, \quad (17)$$

$$\hat{\lambda}_{t\bar{t}W}^{\text{FxFx1j+EW}} = 1.46_{-0.17}^{+0.18}, \quad (18)$$

and are consistent with SM expectations at  $2.7\sigma - 3.0\sigma$ .

While NNLL threshold corrections can improve this picture, direct application of Ref. [20] is hindered by the different scale choices that we assume. That said, taking a comparable correction of  $K_{\text{NNLL-QCD}}^{\text{est}} = \sigma^{\text{NLO+NNLL-QCD}} / \sigma^{\text{NLO-QCD}} = 1.03$ , the associated SM rate and best-fit signal strength are:

$$\sigma_{t\bar{t}W^\pm}^{\text{FxFx1j+EW+NNLL}} = 708 \text{ fb}_{-12\% -1.6\%}^{+12\% +1.6\%}, \quad (19)$$

$$\hat{\lambda}_{t\bar{t}W}^{\text{FxFx1j+EW+NNLL}} = 1.43_{-0.16}^{+0.17}, \quad (20)$$

where we again assume the FxFx uncertainties. With these estimated corrections the discrepancy stays at  $2.7\sigma$ .

To explore the uncertainty associated with our baseline  $(p_T^{j \min}, Q_{\text{cut}}^{\text{FxFx}})$ , we report in the upper panel of table 3 the inclusive  $t\bar{t}W$  cross section at  $\sqrt{s} = 13 \text{ TeV}$  at LO, NLO in QCD,

and with FxFx1j matching for various inputs. Also shown are the  $\mu_f, \mu_r$  scale and PDF uncertainties, and the QCD  $K$ -factor as defined in equation 9. We denote our benchmark rate by  $\dagger$ .

For the inputs considered we observe that NLO multi-jet matching rates span about  $\sigma^{\text{FxFx1j}} \sim 600 \text{ fb} - 670 \text{ fb}$ . This is about 0% – 12% larger than the baseline rate at NLO in QCD in equation 7. Notably, the range of  $\Delta\sigma^{\text{FxFx1j}} \sim 70 \text{ fb}$  is much smaller than the differences in the  $t\bar{t}Wj$  rate at NLO, which span  $\Delta\sigma \sim 250 \text{ fb}$  (see table 1). Naïvely, this indicates a sizable phase space overlap between the  $t\bar{t}W$  and  $t\bar{t}Wj$  processes at NLO in QCD. However, this appears contrary to figure 2, which shows that the characteristic light jet scale in inclusive  $t\bar{t}W$  is well below  $p_T^j = 50 \text{ GeV}$ , and otherwise suggests a much milder phase space overlap for  $p_T^{j\text{min}} \gtrsim 50 \text{ GeV} - 75 \text{ GeV}$ .

As expected [41, 72], we find that the range of FxFx1j predictions is driven by the dependence on the merging scale more than the jet  $p_T$  threshold. In particular, for the largest  $Q_{\text{cut}}^{\text{FxFx}}$  considered the FxFx1j rate reduces to the NLO rate and can be tied to an “over suppression” of the  $t\bar{t}Wj$  multiplicity [74]. To quantify an uncertainty associated with  $Q_{\text{cut}}^{\text{FxFx}}$ , we consider the envelope spanned by all FxFx predictions. For  $Q_{\text{cut}}^{\text{FxFx}} = 70 \text{ GeV} - 350 \text{ GeV}$  and  $p_T^{j\text{min}} = 30 \text{ GeV} - 150 \text{ GeV}$ , we report a variation of  $\delta\sigma^{\text{FxFx1j}}[Q_{\text{cut}}^{\text{FxFx}}]/\sigma_{\text{baseline}}^{\text{FxFx1j}} = \begin{smallmatrix} +2\% \\ -9\% \end{smallmatrix}$ . To quantify an uncertainty associated with  $p_T^{j\text{min}}$ , we fix the merging scale at

$$Q_{\text{cut}}^{\text{FxFx}} = 110 \text{ GeV}, 150 \text{ GeV}, 250 \text{ GeV}, 350 \text{ GeV}, \quad (21)$$

and vary  $p_T^{j\text{min}}$ . For all cases, we find that FxFx rates change only about  $\Delta\sigma^{\text{FxFx1j}}[p_T^{j\text{min}}] \sim 1 \text{ fb} - 10 \text{ fb}$ , or 0.1% – 1.5%.

#### 4. Differential Production

Assuming that the enlarged  $t\bar{t}W$  cross section measurements are solely due to missing QCD corrections, then NLO multi-jet matching cannot be the full picture. At the same time, differences in initial/finite-state radiation, associated production of heavy flavors, and relative enhancements by virtual radiation all impact particle kinematics. Hence, complementary to the total rate itself, kinematic distributions provide a means to test and understand the modeling of inclusive  $t\bar{t}W$  production.

A comprehensive investigation into the impact of NLO multi-jet merging on particle kinematics is beyond our present scope and left to future work. That said, to at least build a qualitative picture, we take as a benchmark the ATLAS analysis [34] associated with the signal strength in equation 4 and consider the  $t\bar{t}W$  decay mode,

$$pp \rightarrow t\bar{t}W^\pm \rightarrow 3W b\bar{b} \rightarrow \ell_i^\pm \ell_j^\pm + X, \quad \ell \in \{e, \mu\}. \quad (22)$$

Here the two same-sign  $W$  bosons decay leptonically and the odd-sign  $W$  decays inclusively. Following closely the selection criteria of table 3 in Ref. [34], then after selection cuts and vetoes, three signal categories are defined:

- The “inclusive selection category” is identified as two same-sign, high- $p_T$  charged leptons  $\ell$ , two reconstructed light jets, and at least one  $b$ -tagged jet.

Order	$p_T^{j\text{min}}$	$Q_{\text{cut}}^{\text{FxFx}}$	$\sigma$ [fb]	$\pm\delta_{\mu_f, \mu_r}$	$\pm\delta_{\text{PDF}}$	$K_{\text{QCD}}$
<b><math>t\bar{t}W^\pm</math> (Inclusive)</b>						
LO	...	...	378	+24%	+2.2%	1.00
NLO	...	...	594	+18%	+2.0%	1.57
FxFx1j	30 GeV	70 GeV	668	+12%	+1.7%	1.12
FxFx1j	30 GeV	110 GeV	656	+12%	+1.7%	1.11
FxFx1j	30 GeV	150 GeV	634	+12%	+1.6%	1.07
FxFx1j	30 GeV	250 GeV	616	+12%	+1.6%	1.04
FxFx1j	30 GeV	350 GeV	596	+12%	+1.6%	1.00
FxFx1j	40 GeV	90 GeV	664	+12%	+1.7%	1.12
FxFx1j	40 GeV	110 GeV	655	+12%	+1.7%	1.10
FxFx1j <sup>†</sup>	50 GeV	110 GeV	655	+12%	+1.6%	1.10
FxFx1j	50 GeV	150 GeV	644	+12%	+1.6%	1.08
FxFx1j	50 GeV	250 GeV	622	+12%	+1.6%	1.05
FxFx1j	50 GeV	350 GeV	602	+12%	+1.7%	1.01
FxFx1j	100 GeV	250 GeV	615	+12%	+1.7%	1.03
FxFx1j	100 GeV	350 GeV	597	+12%	+1.8%	1.00
FxFx1j	150 GeV	350 GeV	597	+12%	+1.8%	1.00
<b><math>t\bar{t}Z</math> (Inclusive)</b>						
LO	...	...	502	+30%	+1.2%	1.00
NLO	...	...	744	+9.5%	+1.1%	1.48
FxFx1j	40 GeV	90 GeV	822	+11%	+1.1%	1.10
FxFx1j <sup>†</sup>	50 GeV	110 GeV	836	+8%	+1.1%	1.12
FxFx1j	100 GeV	250 GeV	820	+12%	+1.2%	1.10
FxFx1j	150 GeV	350 GeV	797	+11%	+1.2%	1.07

Table 3: Upper: At various perturbative orders and ( $p_T^{j\text{min}}, Q_{\text{cut}}^{\text{FxFx}}$ ) assignments with  $|\eta^j| < 4.0$ , the inclusive  $t\bar{t}W$  cross section [fb] at  $\sqrt{s} = 13 \text{ TeV}$ , along with residual scale and PDF uncertainties [%]. Lower: Same for inclusive  $t\bar{t}Z$ . Benchmark FxFx rates denoted by  $\dagger$ .

- The “two same-sign leptons” (2LSS) category assumes category (i) but vetoes events with three or more  $\ell$ .
- The “three leptons” (3L) category again assumes (i) but requires exactly three  $\ell$  with a net charge of  $\pm 1$ .

In figure 3, we plot the differential cross sections at  $\sqrt{s} = 13 \text{ TeV}$  for representative observables and signal categories at NLO in QCD with PS-matching (black) and FxFx-matching (blue). In the insets we plot the ratio of the FxFx and NLO+PS rates. Uncertainty bands are built from the envelope encapsulating the 27-point  $\mu_f, \mu_r, \mu_s$  variation and  $1\sigma$  PDF uncertainty.

Starting with figure 3(a), we show the  $b$ -jet multiplicity ( $N_{b\text{-jets}}$ ) in the inclusive selection category. As anticipated from its larger cross section, we find that the normalization of the FxFx distribution is systematically larger than the NLO+PS one by at least 10%. More specifically, the bin-by-bin normalization grows to about 13% for  $N_{b\text{-jets}} = 2$  and 30% for  $N_{b\text{-jets}} = 3$ , and stems from the opening of  $g^* \rightarrow b\bar{b}$  splitting in  $q\bar{q} \rightarrow t\bar{t}W g^*$  production. While not shown, we report a slight suppression (enhancement) of low (high) light jet multiplicities relative to NLO+PS. Notably, an enhanced rate at high multiplicities for both heavy and light jets is slightly favored by data [34, 35].

For the same signal category, we show in figure 3(b) the  $p_T$  of the same-sign dilepton system ( $p_T^{\ell\ell}$ ). Over the range  $p_T^{\ell\ell} = 0 \text{ GeV} - 200 \text{ GeV}$ , we observe a slowly increasing bin-by-bin shift in the FxFx normalization relative to the NLO+PS normalization, ranging from about a 10% enhancement to about

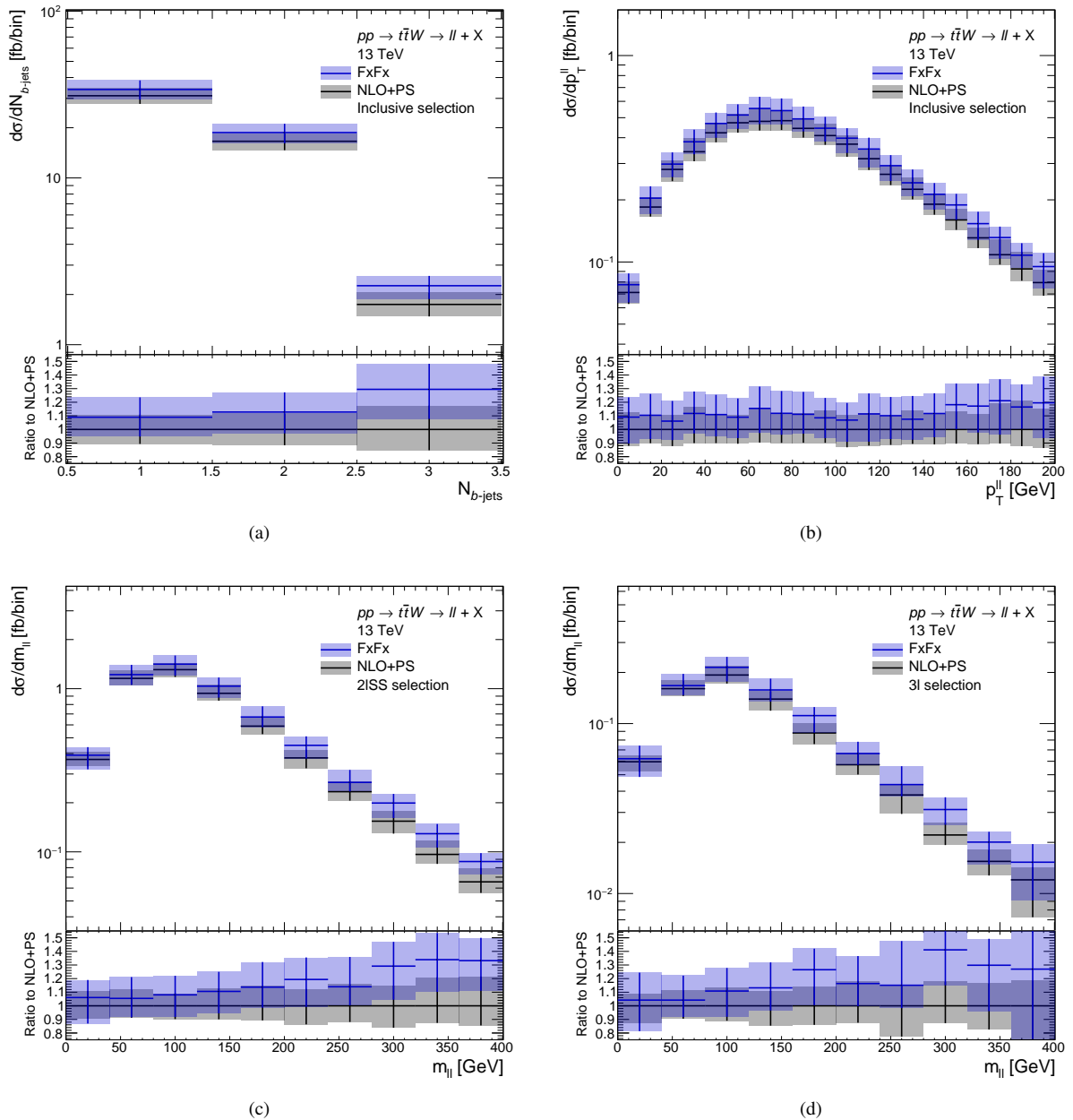


Figure 3: Upper: Differential cross sections with scale and PDF uncertainty envelopes at  $\sqrt{s} = 13$  TeV of the  $pp \rightarrow t\bar{t}W \rightarrow \ell\ell + X$  process at NLO in QCD with PS-matching (dark) and with FxFx matching (light), with respect to the (a)  $b$ -jet multiplicity and (b)  $p_T$  of the same-sign dilepton system in the inclusive selection category, as well as the invariant mass of the dilepton system in the (c) 21SS and (d) 31 categories. Lower: Ratio of FxFx and NLO+PS rates.

20%. We attribute the growing FxFx rate with increasing  $p_T^{\ell\ell}$  to the larger hadronic activity that the dilepton system recoils against, i.e., the positive contributions from the  $O(\alpha_s)$  corrections to the  $t\bar{t}Wj$  sub-channel.

Focusing now on more exclusive signal regions, we plot in figures 3(c) and 3(d), respectively, the invariant mass ( $m_{\ell\ell}$ ) of the same-sign dilepton system for the 21SS and 31 categories. For both categories we observe a qualitatively similar but quantitatively stronger trend than found for  $p_T^{\ell\ell}$ . Numerically, enhancements grow from about 10% to just over 30%,

with the importance of NLO multi-jet matching increasing for larger  $m_{\ell\ell}$ . We argue that the increases at larger  $m_{\ell\ell}$  is due to additional final-state radiation off top quarks in the  $t\bar{t}Wj$  sub-channel at NLO. Such radiation imbue top quarks with recoil momentum that propagate to charged leptons. This in turn leads to larger lepton momenta and thus larger invariant masses.

## 5. Outlook

Due the large impact of QCD radiation at  $O(\alpha_s^4\alpha)$  on the  $t\bar{t}W$  process we are compelled to consider implications for other

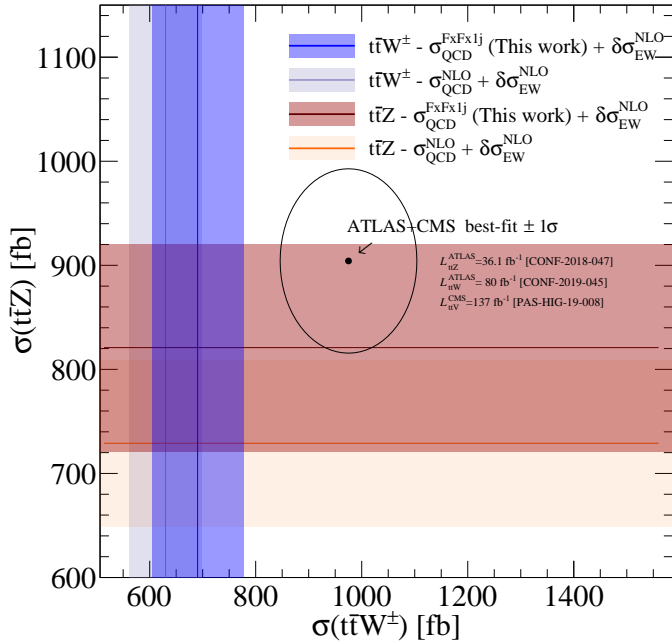


Figure 4: Central cross section predictions at  $\sqrt{s} = 13$  TeV with  $1\sigma$  uncertainty bands for the  $t\bar{t}W$  and  $t\bar{t}Z$  processes at NLO in QCD+EW (light) as well with FxFx matching (dark). Also shown are best-fit measurements from the ATLAS [32, 34] and CMS [36] experiments.

scenarios. This includes, for example, inclusive  $t\bar{t}Z$  production at the LHC, a situation that we now explore.

### 5.1. Inclusive $t\bar{t}Z$ production at the LHC

The SM's  $SU(2)_L$  gauge symmetry dictates that  $t\bar{t}W$  and  $t\bar{t}Z$  production are intimately related. However, due to differences in gauge quantum numbers, inclusive  $t\bar{t}Z$  production occurs via different partonic channels, especially at lowest order. Hence,  $t\bar{t}Z$  possesses a different sensitivity to QCD corrections.

To investigate these differences we repeat the work of section 3 and report in the lower panel of table 3 the cross sections for the  $t\bar{t}Z$  rate at  $O(\alpha_s^2\alpha)$  (LO), up to  $O(\alpha_s^3\alpha)$  (NLO), and FxFx matching up to the first jet multiplicity (FxFx1j) for various inputs. Also reported are the scale and PDF uncertainties, as well as the QCD  $K$ -factor. We observe that QCD corrections generally impact the  $t\bar{t}Z$  process in a comparable manner to the  $t\bar{t}W$  process. More specifically, the NLO and nominal ( $\dagger$ ) FxFx1j  $t\bar{t}Z$  rates possess the  $K$ -factors  $K_{\text{QCD}}^{t\bar{t}Z} = 1.48$  and 1.12, respectively. In comparison, for  $t\bar{t}W$  one finds respectively  $K_{\text{QCD}}^{t\bar{t}W} = 1.57$  and 1.10. For other FxFx inputs we find comparable differences as in  $t\bar{t}W$  but note that the  $t\bar{t}Z$  FxFx1j rate suffers a slightly milder dependence on  $p_T^{\text{min}}$  than  $t\bar{t}W$ .

To summarize our findings, we plot in figure 4 the cross section predictions with uncertainties at  $\sqrt{s} = 13$  TeV for the  $t\bar{t}W$  and  $t\bar{t}Z$  processes at NLO in QCD+EW (light) and FxFx+EW (dark). (For  $t\bar{t}Z$ , we use the EW  $K$ -factor  $K_{\text{NLO-EW}} = 0.98$  [27].) For theoretical uncertainties, we combine scale and PDF uncertainties in quadrature. Also shown is the error-weighted combination of best-fit results from ATLAS [32, 34] and CMS

[36]. Unlike the  $t\bar{t}W$  case, we see appreciable improvement in the agreement between the predicted and measured  $t\bar{t}Z$  rate. However, like the  $t\bar{t}W$  case, there remains a sizable theory uncertainty that prevents a more significant statement.

## 6. Summary and Conclusion

In light of sustained measurements of an enhanced  $t\bar{t}W^\pm$  cross section at the LHC, we report a systematic investigation into the role of the  $t\bar{t}Wj$  and  $t\bar{t}Wjj$  sub-processes in inclusive  $t\bar{t}W$  production. We focus particularly on their impact on total and differential rate normalizations.

To conduct this study we revisited (see section 3.1) the state-of-the-art modeling for inclusive  $t\bar{t}W$  production and took special note of estimated NNLO in QCD corrections that are employed in LHC analyses. Using LO and NLO in QCD computations, we then examined (see section 3.2) the  $t\bar{t}Wj$  and  $t\bar{t}Wjj$  processes. We report that a subset of real and virtual contributions at  $O(\alpha_s^4\alpha)$  in well-defined regions of phase space are positive and can arguably increase the inclusive  $t\bar{t}W$  rate at NLO by at least 10% – 14%. Resummed results at NNLL do not suggest large cancellations against pure two-loop diagrams.

Interestingly, using instead the non-unitary, NLO multi-jet matching scheme FxFx, we find (see section 3.3) that these same QCD corrections at  $O(\alpha_s^4\alpha)$  increase the inclusive  $t\bar{t}W$  cross section at NLO by at most 10% – 12%. We obtain a slightly smaller central normalization for the inclusive  $t\bar{t}W$  production rate than used in LHC analyses, which in turn worsens slightly reported discrepancies. At the same time, after selection cuts and signal categorization, the FxFx description of  $t\bar{t}W$  exhibits enhanced jet multiplicities that are slightly favored by data (see section 4). Our main results are summarized in figure 4. There we compare FxFx-improved cross sections for the  $t\bar{t}W$  and  $t\bar{t}Z$  processes to measurements at  $\sqrt{s} = 13$  TeV.

In conclusion, while production rates at the FxFx1j level do not obviously resolve existing tension between SM predictions and LHC measurements of the  $pp \rightarrow t\bar{t}W + X$  process, the magnitude residual scale uncertainties, the moderate dependence on matching inputs, and the discrepancy with numerical estimates of  $O(\alpha_s^2)$  corrections motivate the need for a full description of inclusive  $t\bar{t}W$  and  $t\bar{t}Z$  production at NNLO in QCD.

## Acknowledgements

We thank Carlos Fibonacci, Fabio Maltoni, Olivier Mattelaer, Aaron Vincent, and Marco Zaro for helpful discussions. We also thank Rikkert Frederix and Ioannis Tsinikos for their careful read of an earlier version of this manuscript.

This work was supported by the Faculty of Science Doctoral Internship Program at the University of the Witwatersrand. This work has also received funding from the European Union's Horizon 2020 research and innovation programme as part of the Marie Skłodowska-Curie Innovative Training Network MC-netITN3 (grant agreement no. 722104), FNRS Excellence of Science EOS be.h Project No. 30820817. SvB and BM are grateful for the continued support from the SA-CERN program

that is supported by the National Research Foundation and the Department of Science and Innovation, and the Research office of the University of the Witwatersrand. RR is supported under the UCLouvain fund MOVE-IN Louvain and acknowledge the contribution of the VBSCan COST Action CA16108.

Computational resources have been provided by the supercomputing facilities of the Université catholique de Louvain (CISM/UCL) and the Consortium des Équipements de Calcul Intensif en Fédération Wallonie Bruxelles (CÉCI) funded by the Fond de la Recherche Scientifique de Belgique (F.R.S.-FNRS) under convention 2.5020.11 and by the Walloon Region.

- [1] G. Aad, et al., Measurement of the  $t\bar{t}W$  and  $t\bar{t}Z$  production cross sections in pp collisions at  $\sqrt{s} = 8$  TeV with the ATLAS detector, JHEP 11 (2015) 172. [arXiv:1509.05276](#), [doi:10.1007/JHEP11\(2015\)172](#).
- [2] V. Khachatryan, et al., Observation of top quark pairs produced in association with a vector boson in pp collisions at  $\sqrt{s} = 8$  TeV, JHEP 01 (2016) 096. [arXiv:1510.01131](#), [doi:10.1007/JHEP01\(2016\)096](#).
- [3] F. del Aguila, J. Aguilar-Saavedra, Distinguishing seesaw models at LHC with multi-lepton signals, Nucl. Phys. B 813 (2009) 22–90. [arXiv:0808.2468](#), [doi:10.1016/j.nuclphysb.2008.12.029](#).
- [4] F. Maltoni, D. Pagani, I. Tsinikos, Associated production of a top-quark pair with vector bosons at NLO in QCD: impact on  $t\bar{t}H$  searches at the LHC, JHEP 02 (2016) 113. [arXiv:1507.05640](#), [doi:10.1007/JHEP02\(2016\)113](#).
- [5] D. de Florian, et al., Handbook of LHC Higgs Cross Sections: 4. Deciphering the Nature of the Higgs Sector 2/2017. [arXiv:1610.07922](#), [doi:10.23731/CYRM-2017-002](#).
- [6] S. Pascoli, R. Ruiz, C. Weiland, Heavy neutrinos with dynamic jet vetoes: multilepton searches at  $\sqrt{s} = 14, 27,$  and 100 TeV, JHEP 06 (2019) 049. [arXiv:1812.08750](#), [doi:10.1007/JHEP06\(2019\)049](#).
- [7] F. Febres Cordero, L. Reina, D. Wackerroth, NLO QCD corrections to W boson production with a massive b-quark jet pair at the Tevatron p anti-p collider, Phys. Rev. D 74 (2006) 034007. [arXiv:hep-ph/0606102](#), [doi:10.1103/PhysRevD.74.034007](#).
- [8] S. Badger, J. M. Campbell, R. Ellis, QCD Corrections to the Hadronic Production of a Heavy Quark Pair and a W-Boson Including Decay Correlations, JHEP 03 (2011) 027. [arXiv:1011.6647](#), [doi:10.1007/JHEP03\(2011\)027](#).
- [9] A. Lazopoulos, T. McElmurry, K. Melnikov, F. Petriello, Next-to-leading order QCD corrections to  $t\bar{t}Z$  production at the LHC, Phys. Lett. B 666 (2008) 62–65. [arXiv:0804.2220](#), [doi:10.1016/j.physletb.2008.06.073](#).
- [10] A. Kardos, Z. Trocsanyi, C. Papadopoulos, Top quark pair production in association with a Z-boson at NLO accuracy, Phys. Rev. D 85 (2012) 054015. [arXiv:1111.0610](#), [doi:10.1103/PhysRevD.85.054015](#).
- [11] J. M. Campbell, R. Ellis,  $t\bar{t}W^{+-}$  production and decay at NLO, JHEP 07 (2012) 052. [arXiv:1204.5678](#), [doi:10.1007/JHEP07\(2012\)052](#).
- [12] M. Garzelli, A. Kardos, C. Papadopoulos, Z. Trocsanyi,  $Z0$  - boson production in association with a top anti-top pair at NLO accuracy with parton shower effects, Phys. Rev. D 85 (2012) 074022. [arXiv:1111.1444](#), [doi:10.1103/PhysRevD.85.074022](#).
- [13] S. Hoeche, F. Krauss, M. Schonherr, F. Siegert, QCD matrix elements + parton showers: The NLO case, JHEP 04 (2013) 027. [arXiv:1207.5030](#), [doi:10.1007/JHEP04\(2013\)027](#).
- [14] M. Garzelli, A. Kardos, C. Papadopoulos, Z. Trocsanyi,  $t\bar{t}W^{+-}$  and  $t\bar{t}Z$  Hadroproduction at NLO accuracy in QCD with Parton Shower and Hadronization effects, JHEP 11 (2012) 056. [arXiv:1208.2665](#), [doi:10.1007/JHEP11\(2012\)056](#).
- [15] J. Alwall, R. Frederix, S. Frixione, V. Hirschi, F. Maltoni, O. Mattelaer, H. S. Shao, T. Stelzer, P. Torrielli, M. Zaro, The automated computation of tree-level and next-to-leading order differential cross sections, and their matching to parton shower simulations, JHEP 07 (2014) 079. [arXiv:1405.0301](#), [doi:10.1007/JHEP07\(2014\)079](#).
- [16] F. Maltoni, M. Mangano, I. Tsinikos, M. Zaro, Top-quark charge asymmetry and polarization in  $t\bar{t}W^{\pm}$  production at the LHC, Phys. Lett. B 736 (2014) 252–260. [arXiv:1406.3262](#), [doi:10.1016/j.physletb.2014.07.033](#).
- [17] I. Tsinikos, Precision top-quark physics at the LHC, Ph.D. thesis, Université Catholique de Louvain (2017). URL <http://hdl.handle.net/2078.1/186371>
- [18] G. Bevilacqua, H.-Y. Bi, H. B. Hartanto, M. Kraus, M. Worek, The simplest of them all:  $t\bar{t}W^{\pm}$  at NLO accuracy in QCD, JHEP 08 (2020) 043. [arXiv:2005.09427](#), [doi:10.1007/JHEP08\(2020\)043](#).
- [19] A. Kulesza, L. Motyka, D. Schwartzler, T. Stebel, V. Theeuwes, Soft gluon resummation for the associated production of a top quark pair with a W boson at the LHC, PoS EPS-HEP2017 (2017) 465. [arXiv:1710.06810](#), [doi:10.22323/1.314.0465](#).
- [20] A. Kulesza, L. Motyka, D. Schwartzler, T. Stebel, V. Theeuwes, Associated production of a top quark pair with a heavy electroweak gauge boson at NLO+NNLL accuracy, Eur. Phys. J. C 79 (3) (2019) 249. [arXiv:1812.08622](#), [doi:10.1140/epjc/s10052-019-6746-z](#).
- [21] A. Kulesza, L. Motyka, D. Schwartzler, T. Stebel, V. Theeuwes, Associated top quark pair production with a heavy boson: differential cross sections at NLO+NNLL accuracy, Eur. Phys. J. C 80 (5) (2020) 428. [arXiv:2001.03031](#), [doi:10.1140/epjc/s10052-020-7987-6](#).
- [22] H. T. Li, C. S. Li, S. A. Li, Renormalization group improved predictions for  $t\bar{t}W^{\pm}$  production at hadron colliders, Phys. Rev. D 90 (9) (2014) 094009. [arXiv:1409.1460](#), [doi:10.1103/PhysRevD.90.094009](#).
- [23] A. Broggio, A. Ferroglia, G. Ossola, B. D. Pecjak, Associated production of a top pair and a W boson at next-to-next-to-leading logarithmic accuracy, JHEP 09 (2016) 089. [arXiv:1607.05303](#), [doi:10.1007/JHEP09\(2016\)089](#).
- [24] A. Broggio, A. Ferroglia, G. Ossola, B. D. Pecjak, R. D. Sameshima, Associated production of a top pair and a Z boson at the LHC to NNLL accuracy, JHEP 04 (2017) 105. [arXiv:1702.00800](#), [doi:10.1007/JHEP04\(2017\)105](#).
- [25] A. Broggio, A. Ferroglia, R. Frederix, D. Pagani, B. D. Pecjak, I. Tsinikos, Top-quark pair hadroproduction in association with a heavy boson at NLO+NNLL including EW corrections, JHEP 08 (2019) 039. [arXiv:1907.04343](#), [doi:10.1007/JHEP08\(2019\)039](#).
- [26] S. Frixione, V. Hirschi, D. Pagani, H. Shao, M. Zaro, Weak corrections to Higgs hadroproduction in association with a top-quark pair, JHEP 09 (2014) 065. [arXiv:1407.0823](#), [doi:10.1007/JHEP09\(2014\)065](#).
- [27] S. Frixione, V. Hirschi, D. Pagani, H. S. Shao, M. Zaro, Electroweak and QCD corrections to top-pair hadroproduction in association with heavy bosons, JHEP 06 (2015) 184. [arXiv:1504.03446](#), [doi:10.1007/JHEP06\(2015\)184](#).
- [28] R. Frederix, D. Pagani, M. Zaro, Large NLO corrections in  $t\bar{t}W^{\pm}$  and  $t\bar{t}\bar{t}$  hadroproduction from supposedly subleading EW contributions, JHEP 02 (2018) 031. [arXiv:1711.02116](#), [doi:10.1007/JHEP02\(2018\)031](#).
- [29] R. Frederix, I. Tsinikos, Subleading EW corrections and spin-correlation effects in  $t\bar{t}W$  multi-lepton signatures [arXiv:2004.09552](#).
- [30] R. Frederix, S. Frixione, V. Hirschi, D. Pagani, H.-S. Shao, M. Zaro, The automation of next-to-leading order electroweak calculations, JHEP 07 (2018) 185. [arXiv:1804.10017](#), [doi:10.1007/JHEP07\(2018\)185](#).
- [31] A. M. Sirunyan, et al., Measurement of the cross section for top quark pair production in association with a W or Z boson in proton-proton collisions at  $\sqrt{s} = 13$  TeV, JHEP 08 (2018) 011. [arXiv:1711.02547](#), [doi:10.1007/JHEP08\(2018\)011](#).
- [32] Measurement of the  $t\bar{t}W$  and  $t\bar{t}Z$  cross sections in proton–proton collisions at  $\sqrt{s} = 13$  TeV with the ATLAS detector. URL <http://cds.cern.ch/record/2639674>
- [33] M. Aaboud, et al., Measurement of the  $t\bar{t}Z$  and  $t\bar{t}W$  cross sections in proton-proton collisions at  $\sqrt{s} = 13$  TeV with the ATLAS detector, Phys. Rev. D 99 (7) (2019) 072009. [arXiv:1901.03584](#), [doi:10.1103/PhysRevD.99.072009](#).
- [34] Analysis of  $t\bar{t}H$  and  $t\bar{t}W$  production in multilepton final states with the ATLAS detector. URL <http://cds.cern.ch/record/2693930>
- [35] Evidence for  $t\bar{t}\bar{t}$  production in the multilepton final state in proton-proton collisions at  $\sqrt{s} = 13$  TeV with the ATLAS detector. URL <http://cds.cern.ch/record/2719519>
- [36] Higgs boson production in association with top quarks in final states with electrons, muons, and hadronically decaying tau leptons at  $\sqrt{s} = 13$  TeV. URL <http://cds.cern.ch/record/2725523>
- [37] S. von Buddenbrock, N. Chakrabarty, A. S. Cornell, D. Kar, M. Kumar, T. Mandal, B. Mellado, B. Mukhopadhyaya, R. G. Reed, X. Ruan, Phenomenological signatures of additional scalar bosons at the LHC, Eur. Phys. J. C 76 (10) (2016) 580. [arXiv:1606.01674](#), [doi:10.1140/](#)

- [epjc/s10052-016-4435-8](#).
- [38] S. von Buddenbrock, A. S. Cornell, A. Fadol, M. Kumar, B. Mellado, X. Ruan, Multi-lepton signatures of additional scalar bosons beyond the Standard Model at the LHC, *J. Phys. G* 45 (11) (2018) 115003. [arXiv:1711.07874](#), [doi:10.1088/1361-6471/aae3d6](#).
- [39] S. Buddenbrock, A. S. Cornell, Y. Fang, A. Fadol Mohammed, M. Kumar, B. Mellado, K. G. Tomiwa, The emergence of multi-lepton anomalies at the LHC and their compatibility with new physics at the EW scale, *JHEP* 10 (2019) 157. [arXiv:1901.05300](#), [doi:10.1007/JHEP10\(2019\)157](#).
- [40] Y. Hernandez, A. S. Cornell, M. Kumar, B. Mellado, X. Ruan, The anomalous production of multi-lepton and its impact on the measurement of  $Wh$  production at the LHC [arXiv:1912.00699](#).
- [41] R. Frederix, S. Frixione, Merging meets matching in MC@NLO, *JHEP* 12 (2012) 061. [arXiv:1209.6215](#), [doi:10.1007/JHEP12\(2012\)061](#).
- [42] S. Frixione, B. R. Webber, Matching NLO QCD computations and parton shower simulations, *JHEP* 06 (2002) 029. [arXiv:hep-ph/0204244](#), [doi:10.1088/1126-6708/2002/06/029](#).
- [43] R. Frederix, S. Frixione, F. Maltoni, T. Stelzer, Automation of next-to-leading order computations in QCD: The FKS subtraction, *JHEP* 10 (2009) 003. [arXiv:0908.4272](#), [doi:10.1088/1126-6708/2009/10/003](#).
- [44] V. Hirschi, R. Frederix, S. Frixione, M. V. Garzelli, F. Maltoni, R. Pittau, Automation of one-loop QCD corrections, *JHEP* 05 (2011) 044. [arXiv:1103.0621](#), [doi:10.1007/JHEP05\(2011\)044](#).
- [45] P. Artoisenet, R. Frederix, O. Mattelaer, R. Rietkerk, Automatic spin-entangled decays of heavy resonances in Monte Carlo simulations, *JHEP* 03 (2013) 015. [arXiv:1212.3460](#), [doi:10.1007/JHEP03\(2013\)015](#).
- [46] J. Alwall, C. Duhr, B. Fuks, O. Mattelaer, D. G. Zdrzalko, C.-H. Shen, Computing decay rates for new physics theories with FeynRules and MadGraph 5\_aMC@NLO, *Comput. Phys. Commun.* 197 (2015) 312–323. [arXiv:1402.1178](#), [doi:10.1016/j.cpc.2015.08.031](#).
- [47] V. Hirschi, O. Mattelaer, Automated event generation for loop-induced processes, *JHEP* 10 (2015) 146. [arXiv:1507.00020](#), [doi:10.1007/JHEP10\(2015\)146](#).
- [48] T. Sjöstrand, S. Ask, J. R. Christiansen, R. Corke, N. Desai, P. Ilten, S. Mrenna, S. Prestel, C. O. Rasmussen, P. Z. Skands, An introduction to PYTHIA 8.2, *Comput. Phys. Commun.* 191 (2015) 159–177. [arXiv:1410.3012](#), [doi:10.1016/j.cpc.2015.01.024](#).
- [49] S. Catani, Y. L. Dokshitzer, M. Seymour, B. Webber, Longitudinally invariant  $K_T$  clustering algorithms for hadron hadron collisions, *Nucl. Phys. B* 406 (1993) 187–224. [doi:10.1016/0550-3213\(93\)90166-M](#).
- [50] S. D. Ellis, D. E. Soper, Successive combination jet algorithm for hadron collisions, *Phys. Rev. D* 48 (1993) 3160–3166. [arXiv:hep-ph/9305266](#), [doi:10.1103/PhysRevD.48.3160](#).
- [51] M. Cacciari, G. P. Salam, G. Soyez, The anti- $k_T$  jet clustering algorithm, *JHEP* 04 (2008) 063. [arXiv:0802.1189](#), [doi:10.1088/1126-6708/2008/04/063](#).
- [52] M. Cacciari, G. P. Salam, Dispelling the  $N^3$  myth for the  $k_T$  jet-finder, *Phys. Lett. B* 641 (2006) 57–61. [arXiv:hep-ph/0512210](#), [doi:10.1016/j.physletb.2006.08.037](#).
- [53] M. Cacciari, G. P. Salam, G. Soyez, FastJet User Manual, *Eur. Phys. J. C* 72 (2012) 1896. [arXiv:1111.6097](#), [doi:10.1140/epjc/s10052-012-1896-2](#).
- [54] J. de Favereau, C. Delaere, P. Demin, A. Giammanco, V. Lematre, A. Mertens, M. Selvaggi, DELPHES 3, A modular framework for fast simulation of a generic collider experiment, *JHEP* 02 (2014) 057. [arXiv:1307.6346](#), [doi:10.1007/JHEP02\(2014\)057](#).
- [55] G. Aad, et al., Electron and photon performance measurements with the ATLAS detector using the 2015–2017 LHC proton-proton collision data, *JINST* 14 (12) (2019) P12006. [arXiv:1908.00005](#), [doi:10.1088/1748-0221/14/12/P12006](#).
- [56] G. Aad, et al., Muon reconstruction performance of the ATLAS detector in proton–proton collision data at  $\sqrt{s}=13\text{TeV}$ , *Eur. Phys. J. C* 76 (5) (2016) 292. [arXiv:1603.05598](#), [doi:10.1140/epjc/s10052-016-4120-y](#).
- [57] G. Aad, et al., ATLAS b-jet identification performance and efficiency measurement with  $t\bar{t}$  events in pp collisions at  $\sqrt{s}=13\text{TeV}$ , *Eur. Phys. J. C* 79 (11) (2019) 970. [arXiv:1907.05120](#), [doi:10.1140/epjc/s10052-019-7450-8](#).
- [58] R. D. Ball, et al., Parton distributions from high-precision collider data, *Eur. Phys. J. C* 77 (10) (2017) 663. [arXiv:1706.00428](#), [doi:10.1140/epjc/s10052-017-5199-5](#).
- [59] A. Buckley, J. Ferrando, S. Lloyd, K. Nordström, B. Page, M. Rfenacht, M. Schnherr, G. Watt, LHAPDF6: parton density access in the LHC precision era, *Eur. Phys. J. C* 75 (2015) 132. [arXiv:1412.7420](#), [doi:10.1140/epjc/s10052-015-3318-8](#).
- [60] J. C. Collins, D. E. Soper, G. F. Sterman, Transverse Momentum Distribution in Drell-Yan Pair and W and Z Boson Production, *Nucl. Phys. B* 250 (1985) 199–224. [doi:10.1016/0550-3213\(85\)90479-1](#).
- [61] J. Collins, *Foundations of perturbative QCD*, Vol. 32, Cambridge University Press, 2013.
- [62] C. Berger, Z. Bern, L. J. Dixon, F. Febres Cordero, D. Forde, T. Gleisberg, H. Ita, D. Kosower, D. Maitre, Next-to-Leading Order QCD Predictions for W+3-Jet Distributions at Hadron Colliders, *Phys. Rev. D* 80 (2009) 074036. [arXiv:0907.1984](#), [doi:10.1103/PhysRevD.80.074036](#).
- [63] J. Campbell, J. Huston, F. Krauss, *The Black Book of Quantum Chromodynamics: A Primer for the LHC Era*, Oxford University Press, 2017.
- [64] C. Degrande, O. Mattelaer, R. Ruiz, J. Turner, Fully-Automated Precision Predictions for Heavy Neutrino Production Mechanisms at Hadron Colliders, *Phys. Rev. D* 94 (5) (2016) 053002. [arXiv:1602.06957](#), [doi:10.1103/PhysRevD.94.053002](#).
- [65] B. Abbott, et al., Differential cross section for W boson production as a function of transverse momentum in  $p\bar{p}$  collisions at  $\sqrt{s}=1.8\text{TeV}$ , *Phys. Lett. B* 513 (2001) 292–300. [arXiv:hep-ex/0010026](#), [doi:10.1016/S0370-2693\(01\)00628-1](#).
- [66] M. Dasgupta, G. Salam, Resummation of nonglobal QCD observables, *Phys. Lett. B* 512 (2001) 323–330. [arXiv:hep-ph/0104277](#), [doi:10.1016/S0370-2693\(01\)00725-0](#).
- [67] J. R. Forshaw, A. Kyrieleis, M. Seymour, Super-leading logarithms in non-global observables in QCD, *JHEP* 08 (2006) 059. [arXiv:hep-ph/0604094](#), [doi:10.1088/1126-6708/2006/08/059](#).
- [68] Monte Carlo Generators for the Production of a W or Z/ $\gamma^*$  Boson in Association with Jets at ATLAS in Run 2. URL <http://cds.cern.ch/record/2120133>
- [69] V. Khachatryan, et al., Measurement of differential cross sections for top quark pair production using the lepton+jets final state in proton-proton collisions at 13 TeV, *Phys. Rev. D* 95 (9) (2017) 092001. [arXiv:1610.04191](#), [doi:10.1103/PhysRevD.95.092001](#).
- [70] M. Aaboud, et al., Measurements of Higgs boson properties in the diphoton decay channel with  $36\text{fb}^{-1}$  of  $pp$  collision data at  $\sqrt{s}=13\text{TeV}$  with the ATLAS detector, *Phys. Rev. D* 98 (2018) 052005. [arXiv:1802.04146](#), [doi:10.1103/PhysRevD.98.052005](#).
- [71] A. M. Sirunyan, et al., Measurement of differential cross sections for Z boson production in association with jets in proton-proton collisions at  $\sqrt{s}=13\text{TeV}$ , *Eur. Phys. J. C* 78 (11) (2018) 965. [arXiv:1804.05252](#), [doi:10.1140/epjc/s10052-018-6373-0](#).
- [72] R. Frederix, S. Frixione, A. Papaefstathiou, S. Prestel, P. Torrielli, A study of multi-jet production in association with an electroweak vector boson, *JHEP* 02 (2016) 131. [arXiv:1511.00847](#), [doi:10.1007/JHEP02\(2016\)131](#).
- [73] S. Catani, F. Krauss, R. Kuhn, B. Webber, QCD matrix elements + parton showers, *JHEP* 11 (2001) 063. [arXiv:hep-ph/0109231](#), [doi:10.1088/1126-6708/2001/11/063](#).
- [74] K. Hamilton, P. Nason, C. Oleari, G. Zanderighi, Merging H/W/Z + 0 and 1 jet at NLO with no merging scale: a path to parton shower + NNLO matching, *JHEP* 05 (2013) 082. [arXiv:1212.4504](#), [doi:10.1007/JHEP05\(2013\)082](#).